

Subcycle resolved strong-field tunneling ionization: Identification of magnetic dipole and electric quadrupole effects

Xiaodan Mao,¹ Hongcheng Ni,^{1,2,3,4,*} Xiaochun Gong,^{1,3} Joachim Burgdörfer,² and Jian Wu^{1,3,4,5,†}

¹State Key Laboratory of Precision Spectroscopy, East China Normal University, Shanghai 200241, China

²Institute for Theoretical Physics, Vienna University of Technology, 1040 Vienna, Austria

³Collaborative Innovation Center of Extreme Optics, Shanxi University, Taiyuan, Shanxi 030006, China

⁴NYU-ECNU Joint Institute of Physics, New York University at Shanghai, Shanghai 200062, China

⁵CAS Center for Excellence in Ultra-intense Laser Science, Shanghai 201800, China

Interaction of a strong laser pulse with matter transfers not only energy but also linear momentum of the photons. Recent experimental advances have made it possible to detect the small amount of linear momentum delivered to the photoelectrons in strong-field ionization of atoms. Linear momentum transfer is a unique signature of the laser-atom interaction beyond its dipolar limit. Here, we present a decomposition of the subcycle time-resolved linear momentum transfer in term of its multipolar components. We show that the magnetic dipole contribution dominates the linear momentum transfer during the dynamical tunneling process while the post-ionization longitudinal momentum transfer in the field-driven motion of the electron in the continuum is primarily governed by the electric quadrupole interaction. Alternatively, exploiting the radiation gauge, we identify nondipole momentum transfer effects that scale either linearly or quadratically with the coupling to the laser field. The present results provide detailed insights into the physical mechanisms underlying the subcycle linear momentum transfer induced by nondipole effects.

I. INTRODUCTION

Tunneling ionization is the first step of many strong-field phenomena and is one of the cornerstones of strong-field and attosecond physics. Tunneling ionization from atoms and molecules is typically described within the electric dipole approximation, where the laser field is considered homogeneous along its propagation direction, thereby neglecting the photon momentum and the field retardation [1]. The dipole approximation holds well for typical parameters of experimental table-top laser setups. In turn, nondipole effects, which result in asymmetric photoelectron momentum distributions about zero along the field propagation direction, are typically very small.

With advances in the detection technology, such weak nondipole effects have recently become accessible [2, 3]. In 2011, *Smeenk et al.* [4] experimentally observed the linear momentum transfer for tunneling ionization of argon and neon. Since then, nondipole tunneling effects have attracted considerable attention. It has been found to cause a negative shift in the photoelectron momentum distribution for linear polarization due to its interplay with the Coulomb field [5]. Remarkably, for nonsequential double ionization, the sum of the nondipole momentum shifts of the two electrons is opposite to the case of single ionization and considerably larger [6]. The nondipole momentum shift follows the prediction of the classical model for low photoelectron energies [7], while for high-order above-threshold ionization, the nondipole momentum shift is found to be substantially modified by large-angle rescattering of the electron [8, 9]. Nondipole effects also play an observable role during the under-barrier tunneling ionization [10, 11]. Moreover, nondipole effects induce a modifica-

tion to the ponderomotive potential thereby shifting the center of the energy rings in the above-threshold ionization [12–14]. In 2019, the pioneering experimental work of *Willenberg et al.* [15] studied the subcycle linear momentum transfer with an attoclock protocol [16, 17], and found a counterintuitive local minimum of the transferred momentum at the peak of the laser electric field. Based on earlier theories of nondipole effects [18–26], we have subsequently developed the theory of subcycle linear momentum transfer [27], which accounts for the interplay between nondipole and nonadiabatic tunneling effects on the sub-optical-cycle time scale.

Different contributions to the linear momentum transfer by nondipole effects can be distinguished. In the time domain, the momentum transfer $\langle p_z \rangle$ along the laser propagation direction (\hat{z}) can be partitioned as [27, 28]

$$\langle p_z \rangle = \langle v_z \rangle + \Delta E/c \quad (1)$$

with $\langle v_z \rangle$ the momentum transfer due to tunneling ionization and $\Delta E/c$ the contribution due to the subsequent continuum motion after tunneling with ΔE denoting the energy gain during the continuum excursion of the electron and c representing the speed of light. An alternative partitioning can be achieved in the energy domain by exploring the influence of different terms of nondipole Hamiltonian to a given order α (α is the fine structure constant) [29–31] on the linear momentum transfer. Recently, the time-integrated contributions of the electric field gradient and the magnetic field to the final momentum distribution in tunneling ionization have been studied [32].

In the present article, we aim at combining the time domain and spectral domain analysis in order to pinpoint the influence of individual nondipole terms in the Hamiltonian on the subcycle time-resolved momentum transfer within a typical attoclock protocol. Employing an elliptically polarized laser pulse, the electrons emitted at different instances of time within an optical cycle are emitted into different directions

* heni@lps.ecnu.edu.cn

† jwu@phy.ecnu.edu.cn

and backscattering is suppressed, which facilitates the subcycle time resolution of nondipole-induced momentum transfer.

The article is organized as follows. In Sec. II, we briefly review the theoretical framework within which we treat the partitioning of the leading-order nondipole corrections in the Hamiltonian for atom-laser interaction. In Sec. III, the subcycle contributions originating from each nondipole Hamiltonian term are analyzed and approximate analytic expressions within the framework of the strong-field approximation (SFA) are given. We present results for the subcycle contributions of the different nondipole interactions in Sec. IV. The time integral momentum transfer as a function of the laser parameters is explored in Sec. V. Conclusions are given in Sec. VI. Atomic units are used throughout unless noted otherwise.

II. THEORETICAL FRAMEWORK

A. The nondipole Hamiltonian

The light wave of a laser in vacuum is a transverse wave with polarization perpendicular to the propagation direction ($\hat{\mathbf{k}}$) along which the linear photon momentum $k = \omega/c$ (ω : laser angular frequency) points. In the following, z is chosen along the laser propagation direction and (x, y) represents the laser polarization plane. For inclusion of nondipole effects into light-matter interactions, the spatio-temporal dependence of the vector potential of the laser field $\mathbf{A}(\mathbf{r}, t) = \mathbf{A}(t - z/c)$ needs to be considered. Focusing in the following on the Hamiltonian operator of an (effective) one-electron atom with atomic potential $V(\mathbf{r})$, the minimal-coupling Hamiltonian in the radiation gauge is given by

$$H = \frac{1}{2} [\mathbf{p} + \mathbf{A}(\mathbf{r}, t)]^2 + V(\mathbf{r}). \quad (2)$$

Since nondipole retardation effects $\sim 1/c$ are the focus of our present study, we have absorbed other $1/c$ factors, in particular those originating from the coupling between charged particles and the radiation field in terms of the fine structure constant α ($\alpha = 1/c$ in atomic units), into the amplitude of the effective vector potential $\mathbf{A}(\mathbf{r}, t)$.

Expanding now the vector potential to first order in c^{-1} , representing field retardation or nondipole effects to lowest order,

$$\mathbf{A}(t - z/c) \approx \mathbf{A}(t) - \frac{z}{c} \dot{\mathbf{A}}(t) = \mathbf{A}(t) + \frac{z}{c} \mathbf{F}(t), \quad (3)$$

with the electric field $\mathbf{F}(t) = -\dot{\mathbf{A}}(t)$, yields the effective Hamiltonian H_{ND} including nondipole effects,

$$H_{\text{ND}} = \frac{1}{2} [\mathbf{p} + \mathbf{A}(t)]^2 + V(\mathbf{r}) + \underbrace{\frac{z}{c} \mathbf{F}(t) \cdot \mathbf{p}}_{\text{F}_1 \text{ term}} + \underbrace{\frac{z}{c} \mathbf{F}(t) \cdot \mathbf{A}(t)}_{\text{F}_2 \text{ term}}, \quad (4)$$

where nondipole retardation effects ($\sim 1/c$) appear both linear ($(z/c) [\mathbf{F}(t) \cdot \mathbf{p}]$) (the F_1 term) and quadratic ($(z/c) [\mathbf{F}(t) \cdot \mathbf{A}(t)]$) (the F_2 term) in the laser field.

Applying now the Powers-Zienau-Wolley gauge transformation

$$\Psi'(\mathbf{r}, t) = e^{i\Lambda_{\text{ND}}(\mathbf{r}, t)} \Psi(\mathbf{r}, t) \quad (5)$$

with the nondipole gauge phase

$$\Lambda_{\text{ND}}(\mathbf{r}, t) = \int_0^1 \mathbf{r} \cdot \mathbf{A}(t - \lambda \frac{z}{c}) d\lambda, \quad (6)$$

the transformed Hamiltonian

$$H'_{\text{ND}} = e^{i\Lambda_{\text{ND}}} (H_{\text{ND}} - i\partial_t) e^{-i\Lambda_{\text{ND}}} \quad (7)$$

becomes [29, 31]

$$H'_{\text{ND}} = \frac{\mathbf{p}^2}{2} + V(\mathbf{r}) + \underbrace{\mathbf{r} \cdot \mathbf{F}(t)}_{\text{E}_1 \text{ term}} + \underbrace{\frac{1}{2c} \mathbf{L} \cdot \mathbf{B}(t)}_{\text{M}_1 \text{ term}} - \underbrace{\frac{z}{2c} [\mathbf{r} \cdot \dot{\mathbf{F}}(t)]}_{\text{E}_2 \text{ term}} \quad (8)$$

with angular momentum $\mathbf{L} = \mathbf{r} \times \mathbf{p}$ and the effective magnetic field $\mathbf{B}(t) = \hat{\mathbf{k}} \times \mathbf{F}(t)$. Eq. (8) represents the multipole expansion of the Hamiltonian, H'_{ND} , including the electric (E_1) and magnetic dipole (M_1) and electric quadrupole (E_2) contributions. The properties of these particle-radiation-field interaction terms are well understood within the framework of lowest order perturbation theory. We explore in the following the role of the terms beyond the standard dipole (E_1) approximation in strong-field ionization and, in particular, in nonadiabatic tunneling ionization.

To study the contribution of individual nondipole terms separately, we will consider also reduced Hamiltonians where only selected nondipole terms are kept,

$$H_{M_1} = \frac{\mathbf{p}^2}{2} + V(\mathbf{r}) + \mathbf{r} \cdot \mathbf{F}(t) + \frac{1}{2c} \mathbf{L} \cdot \mathbf{B}(t), \quad (9)$$

$$H_{E_2} = \frac{\mathbf{p}^2}{2} + V(\mathbf{r}) + \mathbf{r} \cdot \mathbf{F}(t) - \frac{z}{2c} [\mathbf{r} \cdot \dot{\mathbf{F}}(t)]. \quad (10)$$

An analogous decomposition can also be performed for the Hamiltonian in the radiation gauge [Eq. (4)]. Accordingly, we will consider reduced Hamiltonians which include nondipole terms F_1 and F_2 ,

$$H_{F_1} = \frac{1}{2} [\mathbf{p} + \mathbf{A}(t)]^2 + V(\mathbf{r}) + \frac{z}{c} \mathbf{F}(t) \cdot \mathbf{p}, \quad (11)$$

$$H_{F_2} = \frac{1}{2} [\mathbf{p} + \mathbf{A}(t)]^2 + V(\mathbf{r}) + \frac{z}{c} \mathbf{F}(t) \cdot \mathbf{A}(t). \quad (12)$$

For each of these reduced Hamiltonians [Eqs. (9–12)], a suitable gauge transformation analogous to Eqs. (5–7) will be performed.

B. Nondipole strong-field approximation

We focus in the following on the momentum transfer $\langle p_z \rangle$ along the laser propagation direction as the characteristic signature of nondipole effects in strong-field ionization. In a recent publication [27], we have shown by a comparison between the full numerical TDSE solution and the SFA that

for strong-field ionization within an attoclock scenario with elliptically or circularly polarized radiation, the atomic (or Coulomb) potential $V(r)$ [Eqs. (4,8)] has only negligible influence on $\langle p_z \rangle$ as rescattering and laser-Coulomb coupling are suppressed. Consequently, we investigate the contributions of the different nondipole terms to $\langle p_z \rangle$ within the SFA. Moreover, by applying a saddle-point approximation (SPA), we can extract approximate analytic expressions for these nondipole contributions.

Within the SPA including nondipole corrections, labeled ndSPA in the following, the triply differential transition rate to the final state with momentum \mathbf{p} is given by [33–35]

$$W_{\text{ndSPA}}(\mathbf{p}) = |\dot{S}|^{-\alpha_Z} \exp\{2\text{Im}S\}, \quad (13)$$

where $\alpha_Z = 1 + Z/\sqrt{2I_p}$ with Z the asymptotic charge of the remaining ion and I_p the ionization potential, S denotes the nondipole action,

$$S = \int_{t_s}^{t_r} (H_{\text{ND}} + I_p) dt, \quad (14)$$

where H_{ND} presents the Hamiltonian including nondipole terms in various gauges but not the Coulomb potential, and

$$\dot{S} = H_{\text{ND}} + I_p = 0 \quad (15)$$

is the corresponding saddle-point equation. Eq. (15) determines the complex saddle-point time $t_s = t_r + it_i$. The real part of t_s represents the ionization time t_r , the instant the tunneling electron becomes free, while the imaginary part t_i is related to the tunneling rate. For the numerical results presented in the following we use $\alpha_Z = 1$, its exact value only plays a minor role and does not change the conclusions.

For the determination of the linear momentum transfer at the tunneling exit $\langle v_z \rangle$ and the asymptotic momentum transfer $\langle p_z \rangle$, it is advantageous to make a coordinate transformation $(p_x, p_y, p_z) \rightarrow (t_r, k_\perp, p_z)$. With the proper choice of the auxiliary momentum k_\perp (the subscript \perp denotes variables in the laser polarization plane), one of the two saddle-point equations, $\text{Im}\dot{S} = 0$, can be automatically fulfilled. Consequently, the search for the saddle-point time t_s in the complex plane can be reduced to the search along one axis, thereby greatly reducing the computational cost. The choice of k_\perp will depend on H_{ND} as specified below. The auxiliary transverse momentum k_\perp turns out to be closely related to the transverse momentum v_\perp at the tunnel exit. The transition rate \tilde{w} as a function of t_r , k_\perp , and p_z includes the Jacobian of the coordinate transformation

$$\tilde{w}_{\text{ndSPA}}(t_r, k_\perp, p_z) = \left| \det \frac{\partial(p_x, p_y, p_z)}{\partial(t_r, k_\perp, p_z)} \right| W_{\text{ndSPA}}(\mathbf{p}). \quad (16)$$

The expectation value of the subcycle time-resolved linear momentum transfer at the tunnel exit follows as

$$\langle v_z(t_r) \rangle = \frac{\int dk_\perp dp_z v_z(t_r, k_\perp, p_z) \tilde{w}_{\text{ndSPA}}(t_r, k_\perp, p_z)}{\int dk_\perp dp_z \tilde{w}_{\text{ndSPA}}(t_r, k_\perp, p_z)}, \quad (17)$$

and consequently the asymptotic longitudinal momentum $\langle p_z(t_r) \rangle$ as [27, 28]

$$\langle p_z(t_r) \rangle = \langle v_z(t_r) \rangle + \frac{\Delta E}{c}, \quad (18)$$

with $\Delta E = (\langle p_\perp^2 \rangle - \langle v_\perp^2 \rangle)/2$. More generally, the coordinate transformation $(p_x, p_y, p_z) \rightarrow (t_r, k_\perp, p_z)$ allows to determine also other variables of interest as a function of the tunneling ionization time t_r , thereby unraveling information on quantum dynamics along the time axis. Results obtained using Eq. (16) are labeled ndSPA in what follows.

C. Nonadiabatic expansion

Elementary strong-field tunneling theory often referred to as the simple man's model relies on the adiabatic limit of vanishingly small Keldysh parameter γ in which the strong field is treated as quasistatic. Consequently, the tunneling barrier is considered to be time independent and tunneling transitions are ‘‘horizontal’’ and energy conserving. For small but finite Keldysh parameter $\gamma \approx \omega t_i$ nonadiabatic corrections to the quasistatic tunneling process should be accounted for. To determine lowest-order nonadiabatic corrections, we expand the vector potential $\mathbf{A}(t_s) = \mathbf{A}(t_r + it_i)$ up to the second order in t_i [27, 36–41],

$$\mathbf{A}(t_r + it_i) \approx \mathbf{A}(t_r) - it_i \mathbf{F}(t_r) + \frac{1}{2} t_i^2 \dot{\mathbf{F}}(t_r). \quad (19)$$

Restricting the inclusion of nonadiabatic corrections to this order [Eq. (19)] allows the fully analytic evaluation of ionization rate [Eq. (16)]. The results obtained in this approach are hereafter labeled as nondipole saddle-point approximation with nonadiabatic expansion (ndSPANE). We note that this inclusion of nonadiabatic effects is sometimes referred to as the adiabatic expansion [40, 41]. It should be further noted that the k_\perp determined through Eq. (15) may differ from each other when the ndSPA and ndSPANE are used. These deviations do not significantly affect the numerical results.

III. EVALUATION OF THE NONDIPOLE STRONG-FIELD APPROXIMATION

In this section, we apply the ndSPA and the ndSPANE, as outlined above to the subcycle linear momentum transfer with the goal to identify the contributions from individual nondipole terms in the Hamiltonian [Eqs. (4) and (8)]. We first demonstrate the evaluation for full H_{ND} in the radiation gauge [Eq. (4)]. The analogous evaluation for the alternative decompositions of H_{ND} are given in the Appendix.

We first apply a gauge transformation to Eq. (4) with gauge function

$$\Lambda = -\frac{z}{c} \left[\left(\mathbf{p} \cdot \mathbf{A}(t) + \frac{1}{2} A^2(t) \right) \right], \quad (20)$$

which results in [7, 8, 27]

$$H'_{\text{ND}} = \frac{1}{2} \left[\mathbf{p} + \mathbf{A}(t) + \frac{\hat{e}_z}{c} \left(\mathbf{p} \cdot \mathbf{A}(t) + \frac{1}{2} A^2(t) \right) \right]^2 + V \left(\mathbf{r} - \frac{z}{c} \mathbf{A}(t) \right). \quad (21)$$

This gauge transformation implies a time-dependent shift of the origin in the nondipole frame similar to the Kramers-Henneberger gauge. Even when $V(\mathbf{r})$ is eventually neglected in the SFA, such a frame transformation is needed to retrieve quantities in the lab frame from results obtained in this nondipole frame. The corresponding action entering the ndSPA is

$$S = \int_{t_s}^{t_r} \left\{ \frac{1}{2} \left[\mathbf{p} + \mathbf{A}(t) + \frac{\hat{\mathbf{e}}_z}{c} \left(\mathbf{p} \cdot \mathbf{A}(t) + \frac{1}{2} A^2(t) \right) \right]^2 + I_p \right\} dt, \quad (22)$$

and the saddle-point equation reads

$$\frac{1}{2} \left[\mathbf{p} + \mathbf{A}(t_s) + \frac{\hat{\mathbf{e}}_z}{c} \left(\mathbf{p} \cdot \mathbf{A}(t_s) + \frac{1}{2} A^2(t_s) \right) \right]^2 + I_p = 0. \quad (23)$$

With the substitution $\mathbf{k}_\perp = \mathbf{p} + \text{Re} \mathbf{A}(t_s)$, the imaginary part of saddle-point equation becomes

$$\left(1 + \frac{p_z}{c} \right) [k_x \text{Im} A_x(t_s) + k_y \text{Im} A_y(t_s)] = 0. \quad (24)$$

Therefore, by choosing the auxiliary perpendicular momentum k_\perp in the polarization plane as

$$\mathbf{k}_\perp = (\mathbf{p} + \text{Re} \mathbf{A}(t_s)) \cdot \frac{\text{Im} A_y(t_s) \hat{\mathbf{e}}_x - \text{Im} A_x(t_s) \hat{\mathbf{e}}_y}{\sqrt{(\text{Im} A_x(t_s))^2 + (\text{Im} A_y(t_s))^2}}, \quad (25)$$

the imaginary part of the saddle-point equation [Eq. (23)] is automatically fulfilled for arbitrary pulse shapes. The relation between the auxiliary momentum k_\perp [Eq. (25)] and the transverse momentum at the tunnel exit v_\perp will be explored below. Expressing the momentum differential ionization probability $W_{\text{ndSPA}}(\mathbf{p})$ [Eq. (13)] in terms of the coordinates (t_r, k_\perp, p_z) , the time-resolved initial linear momentum $\langle v_z(t_r) \rangle$ is obtained by evaluating Eqs. (16) and (17), and the final linear momentum $\langle p_z(t_r) \rangle$ follows from Eq. (18).

Analytic expressions for $\langle v_z \rangle$ and $\langle p_z \rangle$ can be obtained when keeping only lowest-order nonadiabatic corrections using ndSPANE. Inserting $\mathbf{A}(t_r + it_i)$ [Eq. (19)] into the saddle-point equation [Eq. (15)] and keeping terms up to second order in t_i results in the relationship

$$\mathbf{k}_\perp \cdot \mathbf{F}(t_r) = [\mathbf{p}_\perp + \mathbf{A}(t_r)] \cdot \mathbf{F}(t_r) = 0, \quad (26)$$

i.e., the transverse momentum \mathbf{k}_\perp is orthogonal to the attoclock field at the instant of tunneling ionization t_r . The real part of the saddle-point equation leads to

$$t_i = \sqrt{\frac{k_\perp^2 + 2I_p + p_z^2 + \frac{p_z}{c} (2\mathbf{k}_\perp \cdot \mathbf{A}(t_r) - A^2(t_r))}{\left(1 + \frac{p_z}{c}\right) \tilde{F}^2(t_r)}}, \quad (27)$$

with the effective field $\tilde{F}(t_r) = \sqrt{F^2(t_r) - \mathbf{k}_\perp \cdot \dot{\mathbf{F}}(t_r)}$. The above expression of t_i explicitly defines an effective Keldysh parameter $\gamma_{\text{eff}} = \omega t_i$, which should be small in the tunneling regime. The ionization rate \tilde{w}_{ndSPA} [Eq. (16)] is now obtained

by evaluating the exponential factor

$$\begin{aligned} 2 \text{Im} S &= -2I_p t_i - \text{Re} \int_0^{t_i} \left[\mathbf{p} + \mathbf{A}(t_r + it) \right. \\ &\quad \left. + \frac{\hat{\mathbf{e}}_z}{c} \left(\mathbf{p} \cdot \mathbf{A}(t_r + it) + \frac{1}{2} A^2(t_r + it) \right) \right]^2 dt \\ &\approx -\frac{2}{3\tilde{F}} \left[k_\perp^2 + 2I_p + \left(p_z \right. \right. \\ &\quad \left. \left. - \left(\frac{-2\mathbf{k}_\perp \cdot \mathbf{A} + A^2}{2c} + \frac{2I_p + k_\perp^2}{6c} \right) \right) \right]^2 \frac{3}{2}, \quad (28) \end{aligned}$$

the preexponential prefactor

$$\begin{aligned} |\dot{S}|^{-\alpha_Z} &\approx \left| -i \left(1 + \frac{p_z}{c} \right) t_i \tilde{F}^2 \right|^{-\alpha_Z} \\ &\approx \left[(k_\perp^2 + 2I_p) \tilde{F}^2 \right]^{-\frac{\alpha_Z}{2}} \exp \left\{ -\frac{\alpha_Z p_z}{2c} \right\} \\ &\quad \times \exp \left\{ -\frac{\alpha_Z}{2} \frac{\left(p_z - \frac{-2\mathbf{k}_\perp \cdot \mathbf{A} + A^2}{2c} \right)^2}{k_\perp^2 + 2I_p} \right\}, \quad (29) \end{aligned}$$

and the Jacobian

$$\left| \det \frac{\partial (p_x, p_y, p_z)}{\partial (t_r, k_\perp, p_z)} \right| \approx |F_d + F(t_r)|, \quad (30)$$

where $F_d = k_\perp [F_x(t_r) F_y'(t_r) - F_x'(t_r) F_y(t_r)] / F^2(t_r)$.

Rearranging these expressions, we find

$$\begin{aligned} \tilde{w}_{\text{ndSPANE}} &\approx |F_d + F(t_r)| \left[(k_\perp^2 + 2I_p) \tilde{F}^2 \right]^{-\alpha_Z/2} \\ &\quad \times \exp \left\{ -\frac{2}{3\tilde{F}} \left[k_\perp^2 + 2I_p + \left(1 + \frac{\alpha_Z \tilde{F}}{2(k_\perp^2 + 2I_p)^{3/2}} \right) \right. \right. \\ &\quad \left. \left. \times (p_z - \langle p_z(t_r, k_\perp) \rangle) \right]^2 \frac{3}{2} \right\}, \quad (31) \end{aligned}$$

where

$$\begin{aligned} \langle p_z(t_r, k_\perp) \rangle &= \frac{2I_p + k_\perp^2}{6c} \left[1 - \frac{2\alpha_Z \tilde{F}}{(2I_p + k_\perp^2)^{3/2}} \right] + \frac{-2\mathbf{k}_\perp \cdot \mathbf{A} + A^2}{2c} \\ &\approx \frac{2I_p + k_\perp^2}{6c} \left[1 - \frac{2\alpha_Z F}{(2I_p)^{3/2}} \right] + \frac{-2\mathbf{k}_\perp \cdot \mathbf{A} + A^2}{2c} \quad (32) \end{aligned}$$

with the ponderomotive energy gain ΔE ,

$$\frac{\Delta E}{c} = \frac{p_\perp^2 - k_\perp^2}{2c} = \frac{-2\mathbf{k}_\perp \cdot \mathbf{A} + A^2}{2c}. \quad (33)$$

$\langle v_z(t_r, k_\perp) \rangle$ follows from Eq. (32) as

$$\begin{aligned} \langle v_z(t_r, k_\perp) \rangle &= \langle p_z(t_r, k_\perp) \rangle - \frac{\Delta E}{c} \\ &\approx \frac{2I_p + k_\perp^2}{6c} \left[1 - \frac{2\alpha_Z F(t_r)}{(2I_p)^{3/2}} \right]. \quad (34) \end{aligned}$$

The relation between k_{\perp} and the transverse momentum at the tunnel exit v_{\perp} results from the frame transformation implied by the gauge transformation [Eqs. (20,21)],

$$\mathbf{r}_{\text{lab}} = \mathbf{r} - \frac{z}{c} \mathbf{A}(t_r). \quad (35)$$

Accordingly, we find for the velocities

$$\mathbf{v}_{\text{lab}} = \mathbf{v} - \frac{v_z}{c} \mathbf{A}(t_r) + \frac{z}{c} \mathbf{F}(t_r), \quad (36)$$

while $\mathbf{v}_{\perp} = \mathbf{p}_{\perp} + \mathbf{A}(t_r) + p_z/c \mathbf{A}(t_r)$ follows from Heisenberg's equations of motion for H'_{ND} [Eq. (21)]. Using $z \approx 0$ at the tunnel exit, we have

$$\mathbf{v}_{\perp, \text{lab}} \approx \mathbf{p}_{\perp} + \mathbf{A}(t_r) = \mathbf{k}_{\perp}. \quad (37)$$

Hence, the mean initial linear momentum in the lab frame can be rewritten as

$$\langle v_z(t_r, v_{\perp}) \rangle \approx \frac{2I_p + v_{\perp}^2}{6c} \left[1 - \frac{2\alpha_z F(t_r)}{(2I_p)^{3/2}} \right], \quad (38)$$

where we have dropped the subscript ‘‘lab’’, and the corresponding asymptotic linear momentum as

$$\begin{aligned} \langle p_z(t_r, v_{\perp}) \rangle &= \langle v_z(t_r, v_{\perp}) \rangle + \frac{\Delta E}{c}, \\ &= \langle v_z(t_r, v_{\perp}) \rangle + \frac{p_{\perp}^2 - v_{\perp}^2}{2c}. \end{aligned} \quad (39)$$

The derivation of analogous expressions for $\langle p_z \rangle$ and $\langle v_z \rangle$ predicted by the various approximate Hamiltonian operators [Eqs. (9–12)] containing selected nondipole terms is given in the Appendix.

The results of the expectation value of the linear momentum in the lab frame for different Hamiltonian are summarized in Table I in the Appendix, where we present the asymptotic linear momentum transfer $\langle p_z(t_r, v_{\perp}) \rangle$ [Eq. (39)], which is composed of the initial linear momentum at the tunnel exit $\langle v_z(t_r, v_{\perp}) \rangle$ [Eq. (38)] and $\Delta E/c$ for the continuum motion after tunneling. From Table I, it is obvious that

$$\langle v_z(t_r, v_{\perp}) \rangle_{M_1} + \langle v_z(t_r, v_{\perp}) \rangle_{E_2} = \langle v_z(t_r, v_{\perp}) \rangle, \quad (40)$$

$$\frac{\Delta E_{M_1}}{c} + \frac{\Delta E_{E_2}}{c} = \frac{\Delta E}{c}, \quad (41)$$

$$\langle v_z(t_r, v_{\perp}) \rangle_{F_1} + \langle v_z(t_r, v_{\perp}) \rangle_{F_2} = \langle v_z(t_r, v_{\perp}) \rangle, \quad (42)$$

$$\frac{\Delta E_{F_1}}{c} + \frac{\Delta E_{F_2}}{c} = \frac{\Delta E}{c}, \quad (43)$$

i.e., the sum of the nondipole contributions of the reduced Hamiltonians adds up to that of the full nondipole Hamiltonian, regardless of the partitioning and gauge, as expected.

IV. SUBCYCLE CONTRIBUTION OF NONDIPOLE TERMS

In this section, we quantitatively investigate and illustrate the effects of individual nondipole Hamiltonian terms,

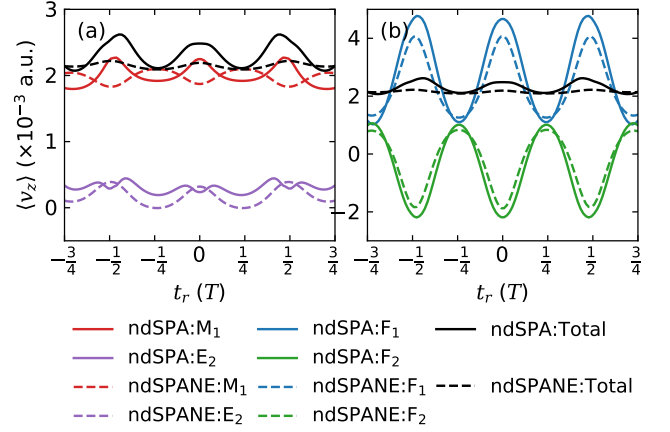


FIG. 1. Subcycle time-resolved linear momentum at the tunnel exit $\langle v_z(t_r) \rangle$ based on the Hamiltonian in the multipole gauge [panel (a)] and in the radiation gauge [panel (b)]. Solid curves are calculated using ndSPA and dashed curves are obtained using ndSPANE. The results of individual nondipole Hamiltonian terms are displayed in different colors. Red curve: the M_1 term, purple curve: the E_2 term, blue curve: the F_1 term, green curve: the F_2 term, black curve: the total nondipole Hamiltonian.

most prominently of the magnetic dipole (M_1) and electric quadrupole (E_2) contributions. To this end, we consider a laser pulse with a vector potential

$$\mathbf{A}(t) = A_0 \cos^4 \left(\frac{\omega t}{2N} \right) \begin{pmatrix} \cos(\omega t + \phi_{\text{CEP}}) \\ \varepsilon \sin(\omega t + \phi_{\text{CEP}}) \end{pmatrix}, \quad (44)$$

with a number N of cycles, $N = 6$, a carrier-envelope phase $\phi_{\text{CEP}} = 0$, pulse ellipticity $\varepsilon = 0.75$, angular frequency $\omega = 0.057$ corresponding to a central wavelength of 800 nm, and the vector potential amplitude A_0 corresponding to a laser peak intensity of 5×10^{14} W/cm². For these laser parameters, the Keldysh parameter is $\gamma \approx 0.8$ corresponding to the (moderate) tunneling regime. In all figures that follow, solid lines represent the results calculated using the ndSPA method and the dashed lines stand for those obtained by the ndSPANE method.

Fig. 1 shows the subcycle time-resolved linear momentum at the tunnel exit $\langle v_z(t_r) \rangle$ caused by various nondipole Hamiltonian terms. Within the multipole gauge [Fig. 1(a)], we find the remarkable results that the magnetic dipole interaction (M_1) strongly dominates the linear momentum transfer during the under-barrier motion while the electric quadrupole interaction (E_2) leaves only an almost negligible footprint on the longitudinal momentum at the tunnel exit. For illustrative purpose we also give the corresponding results for the nondipole contributions of the field-linear (F_1) and field-quadratic (F_2) terms. Here, we find strong oscillations with opposite sign that result in near cancellation of the two contributions. This observation clearly indicates that the decomposition according to the order in coupling with the laser field, unlike the multipole decomposition, does not provide a well-suited starting point for the perturbative expansion of nondipole effects. This is closely related to the fact that the gauge transforma-

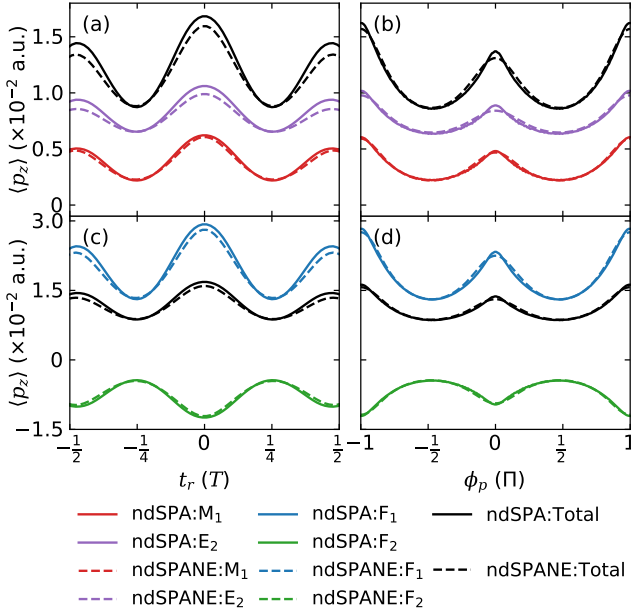


FIG. 2. Subcycle asymptotic linear momentum transfer $\langle p_z \rangle$ as a function of the tunneling exit time t_r (left column) and the attoclock offset angle ϕ_p (right column) in the multipole gauge (upper row) and in the radiation gauge (lower row). The same legend as in Fig. 1 applies.

tion [Eq. (5)] contains field coupling to all orders thereby transforming the Hamiltonian in the radiation gauge [Eq. (4)] which contains terms of first and second order in the field into the multipole Hamiltonian [Eq. (8)], which is strictly linear in the field. We also note that the analytic ndSPANE results for all gauges (Fig. 1) slightly differ from the corresponding full ndSPA calculations on the subcycle level due to the neglect of higher-order corrections in the nonadiabatic expansion $\sim t_i^n$ ($n \geq 3$) [Eq. (19)]. Nevertheless, after summation over the corresponding terms within each gauge, the results closely agree with each other.

Turning now to the asymptotic linear momentum $\langle p_z \rangle$, which is directly experimentally accessible, we display in Fig. 2 the dependence on both the release time t_r (left column) and on the attoclock angle $\phi_p = \arctan(p_y/p_x)$ (right column). Most remarkably, while the electric quadrupole term provides only a negligible contribution to the longitudinal momentum transfer during tunneling ionization (Fig. 1), it dominates over the M_1 contribution in the post-tunneling continuum momentum transfer [Fig. 2(a)]. Moreover, the asymptotic momentum transfer originates predominantly from the field-driven motion in the continuum. The 2ω subcycle oscillations of the momentum transfer during tunneling mediated by the M_1 interaction [Fig. 1(a)] is in phase with the momentum transfer in the continuum, mostly caused by the E_2 term [Figs. 2(a,b)]. By contrast, for the decomposition into the field-linear (F_1) and field-quadratic (F_2) terms of the radiation gauge [Figs. 2(c,d)], the two contribution terms are out of phase by π . Moreover, the F_2 nondipole term induces a momentum transfer due to the nondipole force $-(\mathbf{A} \cdot \mathbf{F})/c$ opposed to that of the laser prop-

agation. Time integration of this force leads to a negative momentum transfer of $-A^2(t_r)/2c$. Regardless of partitioning, summation of the respective individual contributions matches the result of the full nondipole Hamiltonian. Here again, the ndSPANE results agree well with full ndSPA calculations.

V. LASER PARAMETER DEPENDENCE OF THE LINEAR MOMENTUM TRANSFER

In this section, we present results for the laser parameter dependence of the time-integrated linear momentum transfer induced by individual nondipole Hamiltonian terms both at the tunnel exit ($\langle v_z \rangle$) and in the asymptotic region ($\langle p_z \rangle$).

Fig. 3(a) (upper row) shows the dependence of $\langle v_z \rangle$ on the laser ellipticity ε (column 1), wavelength λ (column 2), and peak intensity I_0 (column 3). Fig. 3(b) (lower row) shows the corresponding dependences for $\langle p_z \rangle$. Overall, the under-barrier momentum transfer $\langle v_z \rangle$ is remarkably insensitive to the variation of laser parameters, also the partitioning into M_1 and E_2 changes only marginally with intensity and wavelength which remains fixed when varying the ellipticity. Throughout, the M_1 term strongly dominates over the E_2 term. However, when separating the F_1 and F_2 contributions within the radiation gauge, strong variations as a function of ε can be observed underscoring that this decomposition is not well suited as a starting point for a perturbative expansion.

The asymptotic momentum transfer $\langle p_z \rangle$ (second row) displays a monotonic increase with intensity, wavelength, and ellipticity, in line with the expression

$$\langle p_z \rangle = \langle v_z \rangle + \frac{p_{\perp}^2 - v_{\perp}^2}{2c} \gtrsim \frac{I_p}{3c} + \frac{\varepsilon^2 A_0^2}{2c} = \frac{I_p}{3c} + \frac{\varepsilon^2 F_0^2 \lambda^2}{8\pi^2 c^3}. \quad (45)$$

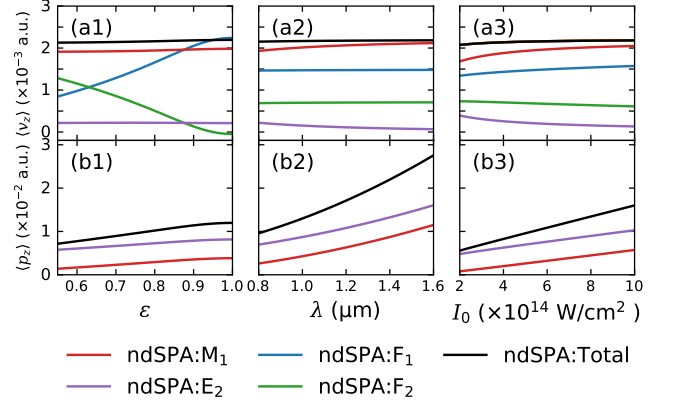


FIG. 3. Linear momentum at the tunnel exit $\langle v_z \rangle$ [upper row (a)] and asymptotic linear momentum $\langle p_z \rangle$ [lower row (b)] induced by M_1 term (red curves), E_2 term (purple curves), F_1 term (blue curves), F_2 term (green curves), and the full nondipole Hamiltonian (black curves) as a function of laser ellipticity ε (column 1), wavelength λ (column 2), and peak intensity I_0 (column 3). Laser parameter in column (1): $\lambda = 800$ nm, $I_0 = 5 \times 10^{14}$ W/cm 2 ; column (2): $\varepsilon = 0.75$, $I_0 = 5 \times 10^{14}$ W/cm 2 ; column (3): $\varepsilon = 0.75$, $\lambda = 800$ nm.

For all laser parameters, the E_2 contribution dominates over the M_1 nondipole contribution to the momentum transfer during the continuum motion and provides, overall, the leading contribution to $\langle p_z \rangle$. The difference between $\langle p_z \rangle$ induced by the E_2 term and that by the M_1 term remains almost constant with a value of about $2I_p/3c$.

VI. CONCLUSIONS

In summary, we have systematically investigated the effect of various distinct nondipole terms in the Hamiltonian describing the coupling of the atomic electron to the radiation field. We consider the subcycle time dependence of strong-field tunneling ionization in an attoclock setting. We include terms to leading order in the field retardation c^{-1} . In the multipole gauge, the magnetic dipole (M_1) interaction and the electric quadrupole (E_2) interaction are accounted for. Alternatively, in the radiation gauge, terms linear (F_1) and quadratic (F_2) in the field strength are considered. The contributions of individual nondipole Hamiltonian terms to the initial linear momentum $\langle v_z \rangle$ at the tunnel exit from the under-barrier motion as well as the asymptotic linear momentum $\langle p_z \rangle$ are studied numerically with the ndSPA method and analytically using the ndSPANE method.

The analysis presented in this work offers novel insights into the nondipole-induced linear momentum on a subcycle time scale. The M_1 magnetic dipole effect plays a dominant role in the under-barrier tunneling process while the E_2 electric quadrupole effect only leaves a small footprint on the initial linear momentum transfer $\langle v_z \rangle$ at the tunnel exit. This trend is largely independent of the laser parameters. In stark contrast to $\langle v_z \rangle$ at the tunnel exit, the E_2 electric quadrupole effect dominates over the M_1 magnetic dipole effect in the asymptotic linear momentum $\langle p_z \rangle$. Each of the nondipole terms induce an oscillation with frequency 2ω in the time-resolved electron emission which arises from the coupling of the nondipole and nonadiabatic tunneling effects. With increasing pulse ellipticity, wavelength, and peak intensity, most of individual nondipole contributions increase.

Regardless of the partitioning and gauge, the sum of individual nondipole contributions equals the results of the full nondipole Hamiltonian, implying a clean separation of individual nondipole effects. The identification of the contributions resulting from individual terms to the momentum transfer opens new avenues for experimentally and theoretically exploring nondipole effects.

ACKNOWLEDGMENTS

This work was supported by the National Key R&D Program of China (Grant No. 2018YFA0306303), the National Natural Science Foundation of China (Grant Nos. 11904103, 92150105, 11834004, 12122404, 11974114), the Austrian Science Fund (Grant Nos. M2692, W1243), and the Science and Technology Commission of Shanghai Municipality (Grant Nos. 21ZR1420100, 19JC1412200, 19560745900).

Appendix A: M_1 term in the multipole gauge

Similar to the derivation of the nondipole effect of the full Hamiltonian, the contribution of the magnetic dipole term can be studied using the Hamiltonian in the multipole gauge containing only the M_1 term

$$H_{M_1} = \frac{1}{2}\mathbf{p}^2 + V(\mathbf{r}) + \mathbf{r} \cdot \mathbf{F}(t) + \frac{1}{2c}\mathbf{L} \cdot \mathbf{B}(t). \quad (\text{A1})$$

We carry out two consecutive gauge transformations with $\Lambda_1 = -\mathbf{A}(t) \cdot \mathbf{r}$ and $\Lambda_2 = -(z/2c)[(\mathbf{p} \cdot \mathbf{A}(t)) + A^2(t)/2] + (p_z/2c)(\mathbf{r} \cdot \mathbf{A}(t))$ to get a new Hamiltonian

$$H'_{M_1} = \frac{1}{2} \left[\mathbf{p} + \mathbf{A}(t) + \frac{\hat{e}_z}{2c} \left(\mathbf{p} \cdot \mathbf{A}(t) + \frac{1}{2}A^2(t) \right) - \frac{p_z}{2c}\mathbf{A}(t) \right]^2 + V \left[\mathbf{r} - \frac{1}{2c} \left(z\mathbf{A}(t) - (\mathbf{r} \cdot \mathbf{A}(t))\hat{e}_z \right) \right], \quad (\text{A2})$$

where the corresponding saddle-point equation is written as

$$\frac{1}{2} \left[\mathbf{p} + \mathbf{A}(t_s) + \frac{\hat{e}_z}{2c} \left(\mathbf{p} \cdot \mathbf{A}(t_s) + \frac{1}{2}A^2(t_s) \right) - \frac{p_z}{2c}\mathbf{A}(t_s) \right]^2 + I_p = 0. \quad (\text{A3})$$

In the ndSPA method, we define

$$\mathbf{k}_\perp = \left[\mathbf{p} + \left(1 - \frac{p_z}{2c} \right) \text{Re} \mathbf{A}(t_s) \right] \cdot \frac{\text{Im}A_y(t_s)\hat{e}_x - \text{Im}A_x(t_s)\hat{e}_y}{\sqrt{(\text{Im}A_x(t_s))^2 + (\text{Im}A_y(t_s))^2}} \quad (\text{A4})$$

to obtain the linear momentum by evaluating Eq. (A3).

In the ndSPANE procedure, we may get

$$t_i = \sqrt{\frac{k_\perp^2 + 2I_p + p_z^2 + \frac{p_z}{c} [\mathbf{k}_\perp \cdot \mathbf{A}(t_r) - \frac{1}{2}A^2(t_r)]}{\left[1 - \frac{p_z}{2c} \left(1 + \frac{\mathbf{k}_\perp \cdot \dot{\mathbf{F}}(t_r)}{F^2(t_r)} \right) \right] \tilde{F}^2(t_r)}}, \quad (\text{A5})$$

where $\mathbf{k}_\perp = \mathbf{p}_\perp + (1 - p_z/2c)\mathbf{A}(t_r)$ with $\mathbf{k}_\perp \cdot \mathbf{F}(t_r) = 0$. Based on the exponential factor

$$\begin{aligned} 2\text{Im}S &= -2I_p t_i - \text{Re} \int_0^{t_i} \left[\mathbf{p} + \mathbf{A}(t_r + it) - \frac{p_z}{2c}\mathbf{A}(t_r + it) \right. \\ &\quad \left. + \frac{\hat{e}_z}{2c} \left(\mathbf{p} \cdot \mathbf{A}(t_r + it) + \frac{1}{2}A^2(t_r + it) \right) \right]^2 dt \\ &\approx -\frac{2}{3\tilde{F}} \left[k_\perp^2 + 2I_p + \left(p_z \right. \right. \\ &\quad \left. \left. - \left(\frac{-\mathbf{k}_\perp \cdot \mathbf{A} + \frac{1}{2}A^2}{2c} - \frac{2I_p + k_\perp^2}{12c} \left(1 + \frac{\mathbf{k}_\perp \cdot \dot{\mathbf{F}}}{\tilde{F}^2} \right) \right) \right]^2 \frac{3}{2}, \quad (\text{A6}) \end{aligned}$$

TABLE I. Subcycle time-resolved contributions of individual nondipole Hamiltonian terms to the initial linear momentum $\langle v_z \rangle$ at the tunnel exit and the asymptotic linear momentum $\langle p_z \rangle$. The full nondipole Hamiltonian H_{ND} is reduced to study the influence of the various nondipole contributions, including the magnetic dipole term M_1 [Eq. (9)], the electric quadrupole term E_2 [Eq. (10)], the field-linear term F_1 [Eq. (11)], and the field-quadratic term F_2 [Eq. (12)]. The asymptotic linear momentum $\langle p_z \rangle$ relates to the one at the tunnel exit $\langle v_z \rangle$ as $\langle p_z \rangle = \langle v_z \rangle + \Delta E/c$, where $\Delta E/c$ originates from the ponderomotive acceleration in the continuum after tunneling. The initial linear momentum $\langle v_z \rangle$ contains five contributions: the under-barrier motion including the nondipole nonadiabatic coupling, the preexponential prefactor, the reduction factor caused by reducing the full nondipole Hamiltonian, the correction Jacobian of the coordinate transformation, and the correction resulting from the transformation from the respective nondipole frame to the lab frame. The table is summarized from Eqs. (38–39,A18–A20,B18–B20,C18–C20,D13–D15).

Terms	tunneling motion $\langle v_z \rangle$					continuum motion $\frac{\Delta E}{c}$
	under-barrier	exp. prefactor	reduction	Jacobian	mapping	
Total	$\frac{2I_p + v_\perp^2}{6c}$		$\times 1$	$+0$	$+0$	$+\frac{p_\perp^2 - v_\perp^2}{2c}$
M_1	$-\frac{2I_p + v_\perp^2}{12c}$	$\times \left[1 - \frac{2\alpha_Z F}{(2I_p)^{3/2}} \right]$	$\times \left(1 + \frac{\mathbf{v}_\perp \cdot \dot{\mathbf{F}}}{F^2} \right)$	$-\frac{F}{4c\sqrt{2I_p}} \frac{F}{F_d + F}$	$+\frac{2I_p + v_\perp^2}{4c} \frac{F^2}{F^2}$	$+\frac{p_\perp^2 - v_\perp^2}{4c} - \frac{2I_p + v_\perp^2}{4c} \frac{F^2}{F^2}$
E_2	$\frac{2I_p + v_\perp^2}{4c}$		$\times \left(1 + \frac{\mathbf{v}_\perp \cdot \dot{\mathbf{F}}}{3F^2} \right)$	$+\frac{F}{4c\sqrt{2I_p}} \frac{F}{F_d + F}$	$-\frac{2I_p + v_\perp^2}{4c} \frac{F^2}{F^2}$	$+\frac{p_\perp^2 - v_\perp^2}{4c} + \frac{2I_p + v_\perp^2}{4c} \frac{F^2}{F^2}$
F_1	$\frac{2I_p + v_\perp^2}{6c}$		$\times \left(-\frac{\mathbf{v}_\perp \cdot \dot{\mathbf{F}}}{F^2} \right)$	$-\frac{F}{2c\sqrt{2I_p}} \frac{F}{F_d + F}$	$-\frac{\mathbf{v}_\perp \cdot \mathbf{A}}{c}$	$-\frac{\mathbf{v}_\perp \cdot \mathbf{A} - A^2}{c}$
F_2	$\frac{2I_p + v_\perp^2}{6c}$		$\times \left(1 + \frac{\mathbf{v}_\perp \cdot \dot{\mathbf{F}}}{F^2} \right)$	$+\frac{F}{2c\sqrt{2I_p}} \frac{F}{F_d + F}$	$+\frac{\mathbf{v}_\perp \cdot \mathbf{A}}{c}$	$-\frac{A^2}{2c}$

the preexponential prefactor

$$\begin{aligned}
|\dot{S}|^{-\alpha_Z} &\approx \left| -i \left[1 - \frac{p_z}{2c} \left(1 + \frac{\mathbf{k}_\perp \cdot \dot{\mathbf{F}}}{\tilde{F}^2} \right) \right] t_i \tilde{F}^2 \right|^{-\alpha_Z} \\
&\approx \left[(k_\perp^2 + 2I_p) \tilde{F}^2 \right]^{-\frac{\alpha_Z}{2}} \exp \left\{ \frac{\alpha_Z}{2} \frac{p_z}{2c} \left(1 + \frac{\mathbf{k}_\perp \cdot \dot{\mathbf{F}}}{\tilde{F}^2} \right) \right\} \\
&\times \exp \left\{ -\frac{\alpha_Z}{2} \frac{\left(p_z - \frac{-\mathbf{k}_\perp \cdot \mathbf{A} + \frac{1}{2}A^2}{2c} \right)^2}{k_\perp^2 + 2I_p} \right\}, \quad (\text{A7})
\end{aligned}$$

and the Jacobian

$$\begin{aligned}
\left| \det \frac{\partial (p_x, p_y, p_z)}{\partial (t_r, k_\perp, p_z)} \right| &\approx |F_d + F(t_r)| \left(1 - \frac{p_z}{2c} \frac{F(t_r)}{F_d + F(t_r)} \right) \\
&\approx |F_d + F(t_r)| \exp \left\{ -\frac{p_z}{2c} \frac{F(t_r)}{F_d + F(t_r)} \right\}, \quad (\text{A8})
\end{aligned}$$

the transition rate is written as

$$\begin{aligned}
\tilde{w}_{\text{ndSPAN}} &\approx |F_d + F(t_r)| \left[(k_\perp^2 + 2I_p) \tilde{F}^2 \right]^{-\alpha_Z/2} \\
&\times \exp \left\{ -\frac{2}{3\tilde{F}} \left[k_\perp^2 + 2I_p + \left(1 + \frac{\alpha_Z \tilde{F}}{2(k_\perp^2 + 2I_p)^{3/2}} \right) \right. \right. \\
&\times \left. \left. (p_z - \langle p_z(t_r, k_\perp) \rangle_{M_1})^2 \right]^{3/2} \right\}, \quad (\text{A9})
\end{aligned}$$

where

$$\begin{aligned}
\langle p_z(t_r, k_\perp) \rangle_{M_1} &= -\frac{2I_p + k_\perp^2}{12c} \left(1 + \frac{\mathbf{k}_\perp \cdot \dot{\mathbf{F}}(t_r)}{\tilde{F}^2(t_r)} \right) \left(1 - \frac{2\alpha_Z \tilde{F}(t_r)}{(2I_p + k_\perp^2)^{3/2}} \right) \\
&\quad - \frac{\tilde{F}(t_r)}{4c\sqrt{2I_p + k_\perp^2}} \frac{F(t_r)}{F_d + F(t_r)} + \frac{-\mathbf{k}_\perp \cdot \mathbf{A} + (1/2)A^2}{2c} \\
&\approx -\frac{2I_p + k_\perp^2}{12c} \left(1 + \frac{\mathbf{k}_\perp \cdot \dot{\mathbf{F}}(t_r)}{F^2(t_r)} \right) \left(1 - \frac{2\alpha_Z F(t_r)}{(2I_p)^{3/2}} \right) \\
&\quad - \frac{F(t_r)}{4c\sqrt{2I_p}} \frac{F(t_r)}{F_d + F(t_r)} + \frac{-\mathbf{k}_\perp \cdot \mathbf{A} + (1/2)A^2}{2c}. \quad (\text{A10})
\end{aligned}$$

According to the Heisenberg's equations of motion for H'_{M_1} [Eq. (A2)],

$$\mathbf{v}_\perp = \mathbf{p}_\perp + \mathbf{A}, \quad (\text{A11})$$

$$v_z = p_z - \frac{1}{2c} \mathbf{v}_\perp \cdot \mathbf{A} + \frac{1}{2c} \left(\mathbf{p}_\perp \cdot \mathbf{A} + \frac{1}{2}A^2 \right), \quad (\text{A12})$$

and the frame transformation,

$$\mathbf{r}_{\text{lab}} = \mathbf{r} - \frac{z}{2c} \mathbf{A} + \frac{\hat{\mathbf{e}}_z}{2c} (\mathbf{r} \cdot \mathbf{A}), \quad (\text{A13})$$

$$\mathbf{v}_{\text{lab}} = \mathbf{v} - \frac{v_z}{2c} \mathbf{A} + \frac{z}{2c} \mathbf{F} + \frac{\hat{\mathbf{e}}_z}{2c} (\mathbf{v}_\perp \cdot \mathbf{A}) - \frac{\hat{\mathbf{e}}_z}{2c} (\mathbf{r} \cdot \mathbf{F}), \quad (\text{A14})$$

we can obtain the velocities in the lab frame,

$$\mathbf{v}_{\perp, \text{lab}} = \mathbf{p}_\perp + \mathbf{A} - \frac{v_z}{2c} \mathbf{A} + \frac{z}{2c} \mathbf{F}, \quad (\text{A15})$$

$$v_{z, \text{lab}} = p_z + \frac{1}{2c} \left(\mathbf{p}_\perp \cdot \mathbf{A} + \frac{1}{2}A^2 \right) - \frac{1}{2c} \mathbf{r} \cdot \mathbf{F}. \quad (\text{A16})$$

At the tunnel exit, using $z \approx 0$ and

$$\begin{aligned} r_0 &= \text{Re} \int_{t_s}^{t_r} \mathbf{v}_\perp dt = \text{Im} \int_0^{t_i} \left(1 - \frac{p_z}{2c}\right) \mathbf{A}(t_r + it) dt \\ &= -\frac{1}{2} t_i^2 \left(1 - \frac{p_z}{2c}\right) \mathbf{F}(t_r) \\ &\approx -\left(1 - \frac{p_z}{2c}\right) \frac{k_\perp^2 + 2I_p}{2} \frac{\mathbf{F}}{\tilde{F}^2}, \end{aligned} \quad (\text{A17})$$

we have $\mathbf{v}_{\perp, \text{lab}} = \mathbf{k}_\perp$, hence the mean initial linear momentum in the lab frame can be rewritten as

$$\begin{aligned} \langle v_z(t_r, v_\perp) \rangle_{M_1} &\approx -\frac{2I_p + v_\perp^2}{12c} \left(1 + \frac{\mathbf{v}_\perp \cdot \dot{\mathbf{F}}(t_r)}{F^2(t_r)}\right) \left(1 - \frac{2\alpha_Z F(t_r)}{(2I_p)^{3/2}}\right) \\ &\quad - \frac{F(t_r)}{4c\sqrt{2I_p}} \frac{F(t_r)}{F_d + F(t_r)} + \frac{2I_p + v_\perp^2}{4c} \frac{F^2(t_r)}{\tilde{F}^2(t_r)}, \end{aligned} \quad (\text{A18})$$

where we have dropped the subscript ‘‘lab’’, with the ponderomotive energy gain ΔE ,

$$\frac{\Delta E_{M_1}}{c} \approx \frac{p_\perp^2 - v_\perp^2}{4c} - \frac{2I_p + v_\perp^2}{4c} \frac{F^2(t_r)}{\tilde{F}^2(t_r)}, \quad (\text{A19})$$

and the corresponding asymptotic linear momentum

$$\begin{aligned} \langle p_z(t_r, v_\perp) \rangle_{M_1} &= \langle v_z(t_r, v_\perp) \rangle_{M_1} + \frac{\Delta E_{M_1}}{c} \\ &= \langle v_z(t_r, v_\perp) \rangle_{M_1} + \frac{p_\perp^2 - v_\perp^2}{4c} - \frac{2I_p + v_\perp^2}{4c} \frac{F^2(t_r)}{\tilde{F}^2(t_r)}. \end{aligned} \quad (\text{A20})$$

The results of Eqs. (A18–A20) are summarized in Table I.

Appendix B: E_2 term in the multipole gauge

The contribution of the electric quadrupole term can be studied using the Hamiltonian in the multipole gauge containing only the E_2 term

$$H_{E_2} = \frac{1}{2} p^2 + V(t) + \mathbf{r} \cdot \mathbf{F}(t) - \frac{z}{2c} [\mathbf{r} \cdot \dot{\mathbf{F}}(t)]. \quad (\text{B1})$$

We carry out two consecutive gauge transformations with gauge phases $\Lambda_1 = -\mathbf{A}(t) \cdot \mathbf{r} - z[\mathbf{r} \cdot \mathbf{F}(t)]/2c$ and $\Lambda_2 = -(z/2c)[(\mathbf{p} \cdot \mathbf{A}(t)) + A^2(t)/2] - (p_z/2c)(\mathbf{r} \cdot \mathbf{A}(t))$ to get a new Hamiltonian

$$\begin{aligned} H'_{E_2} &= \frac{1}{2} \left[\mathbf{p} + \mathbf{A}(t) + \frac{\hat{e}_z}{2c} \left(\mathbf{p} \cdot \mathbf{A}(t) + \frac{1}{2} A^2(t) \right) + \frac{p_z}{2c} \mathbf{A}(t) \right]^2 \\ &\quad + V \left[\mathbf{r} - \frac{1}{2c} \left(z\mathbf{A}(t) + (\mathbf{r} \cdot \mathbf{A}(t)) \hat{e}_z \right) \right], \end{aligned} \quad (\text{B2})$$

where the corresponding saddle-point equation is written as

$$\begin{aligned} \frac{1}{2} \left[\mathbf{p} + \mathbf{A}(t_s) + \frac{\hat{e}_z}{2c} \left(\mathbf{p} \cdot \mathbf{A}(t_s) + \frac{1}{2} A^2(t_s) \right) + \frac{p_z}{2c} \mathbf{A}(t_s) \right]^2 \\ + I_p = 0. \end{aligned} \quad (\text{B3})$$

In the ndSPA method, we define

$$\mathbf{k}_\perp = \left[\mathbf{p} + \left(1 + \frac{p_z}{2c}\right) \text{Re} \mathbf{A}(t_s) \right] \cdot \frac{\text{Im} A_y(t_s) \hat{e}_x - \text{Im} A_x(t_s) \hat{e}_y}{\sqrt{(\text{Im} A_x(t_s))^2 + (\text{Im} A_y(t_s))^2}} \quad (\text{B4})$$

to obtain the linear momentum by evaluating Eq. (B3).

In the ndSPANE procedure, we may get

$$t_i = \sqrt{\frac{k_\perp^2 + 2I_p + p_z^2 + \frac{p_z}{c} [\mathbf{k}_\perp \cdot \mathbf{A}(t_r) - \frac{1}{2} A^2(t_r)]}{\left[1 + \frac{p_z}{2c} \left(3 + \frac{\mathbf{k}_\perp \cdot \dot{\mathbf{F}}(t_r)}{\tilde{F}^2(t_r)}\right)\right] \tilde{F}^2(t_r)}}, \quad (\text{B5})$$

where $\mathbf{k}_\perp = \mathbf{p}_\perp + (1 + p_z/2c)\mathbf{A}(t_r)$, with $\mathbf{k}_\perp \cdot \mathbf{F}(t_r) = 0$. Based on the exponential factor

$$\begin{aligned} 2\text{Im} S &= -2I_p t_i - \text{Re} \int_0^{t_i} \left[\mathbf{p} + \mathbf{A}(t_r + it) + \frac{p_z}{2c} \mathbf{A}(t_r + it) \right. \\ &\quad \left. + \frac{\hat{e}_z}{2c} \left(\mathbf{p} \cdot \mathbf{A}(t_r + it) + \frac{1}{2} A^2(t_r + it) \right) \right]^2 dt \\ &\approx -\frac{2}{3\tilde{F}} \left[k_\perp^2 + 2I_p + \left(p_z \right. \right. \\ &\quad \left. \left. - \left(\frac{-\mathbf{k}_\perp \cdot \mathbf{A} + \frac{1}{2} A^2}{2c} + \frac{2I_p + k_\perp^2}{4c} \left(1 + \frac{\mathbf{k}_\perp \cdot \dot{\mathbf{F}}}{3\tilde{F}^2}\right) \right) \right]^2 \right]^{\frac{3}{2}}, \end{aligned} \quad (\text{B6})$$

the preexponential prefactor

$$\begin{aligned} |\dot{S}|^{-\alpha_Z} &\approx \left| -i \left[1 + \frac{p_z}{2c} \left(3 + \frac{\mathbf{k}_\perp \cdot \dot{\mathbf{F}}}{\tilde{F}^2} \right) \right] t_i \tilde{F}^2 \right|^{-\alpha_Z} \\ &\approx \left[(k_\perp^2 + 2I_p) \tilde{F}^2 \right]^{-\frac{\alpha_Z}{2}} \exp \left\{ -\frac{\alpha_Z}{2} \frac{p_z}{2c} \left(3 + \frac{\mathbf{k}_\perp \cdot \dot{\mathbf{F}}}{\tilde{F}^2} \right) \right\} \\ &\quad \times \exp \left\{ -\frac{\alpha_Z}{2} \frac{\left(p_z - \frac{-\mathbf{k}_\perp \cdot \mathbf{A} + \frac{1}{2} A^2}{2c} \right)^2}{k_\perp^2 + 2I_p} \right\}, \end{aligned} \quad (\text{B7})$$

and the Jacobian

$$\begin{aligned} \left| \det \frac{\partial (p_x, p_y, p_z)}{\partial (t_r, k_\perp, p_z)} \right| &\approx |F_d + F(t_r)| \left(1 + \frac{p_z}{2c} \frac{F(t_r)}{F_d + F(t_r)} \right) \\ &\approx |F_d + F(t_r)| \exp \left\{ \frac{p_z}{2c} \frac{F(t_r)}{F_d + F(t_r)} \right\}, \end{aligned} \quad (\text{B8})$$

the transition rate is written as

$$\begin{aligned} \tilde{w}_{\text{ndSPANE}} &\approx |F_d + F(t_r)| \left[(k_\perp^2 + 2I_p) \tilde{F}^2 \right]^{-\alpha_Z/2} \\ &\quad \times \exp \left\{ -\frac{2}{3\tilde{F}} \left[k_\perp^2 + 2I_p + \left(1 + \frac{\alpha_Z \tilde{F}}{2(k_\perp^2 + 2I_p)^{\frac{3}{2}}} \right) \right. \right. \\ &\quad \left. \left. \times (p_z - \langle p_z(t_r, k_\perp) \rangle_{E_2})^2 \right]^{\frac{3}{2}} \right\}, \end{aligned} \quad (\text{B9})$$

where

$$\begin{aligned} \langle p_z(t_r, k_\perp) \rangle_{E_2} &= \frac{2I_p + k_\perp^2}{4c} \left(1 + \frac{\mathbf{k}_\perp \cdot \dot{\mathbf{F}}(t_r)}{3\tilde{F}^2(t_r)} \right) \left(1 - \frac{2\alpha_Z \tilde{F}(t_r)}{(2I_p + k_\perp^2)^{3/2}} \right) \\ &\quad + \frac{\tilde{F}(t_r)}{4c\sqrt{2I_p + k_\perp^2}} \frac{F(t_r)}{F_d + F(t_r)} + \frac{-\mathbf{k}_\perp \cdot \mathbf{A} + (1/2)A^2}{2c} \\ &\approx \frac{2I_p + k_\perp^2}{4c} \left(1 + \frac{\mathbf{k}_\perp \cdot \dot{\mathbf{F}}(t_r)}{3F^2(t_r)} \right) \left(1 - \frac{2\alpha_Z F(t_r)}{(2I_p)^{3/2}} \right) \\ &\quad + \frac{F(t_r)}{4c\sqrt{2I_p}} \frac{F(t_r)}{F_d + F(t_r)} + \frac{-\mathbf{k}_\perp \cdot \mathbf{A} + (1/2)A^2}{2c}. \end{aligned} \quad (\text{B10})$$

According to the Heisenberg's equations of motion for H'_{E_2} [Eq. (B2)],

$$\mathbf{v}_\perp = \mathbf{p}_\perp + \mathbf{A} + \frac{p_z}{c} \mathbf{A}, \quad (\text{B11})$$

$$v_z = p_z + \frac{1}{2c} \mathbf{v} \cdot \mathbf{A} + \frac{1}{2c} \left(\mathbf{p} \cdot \mathbf{A} + \frac{1}{2}A^2 \right), \quad (\text{B12})$$

and the frame transformation,

$$\mathbf{r}_{\text{lab}} = \mathbf{r} - \frac{z}{2c} \mathbf{A} - \frac{\hat{e}_z}{2c} (\mathbf{r} \cdot \mathbf{A}), \quad (\text{B13})$$

$$\mathbf{v}_{\text{lab}} = \mathbf{v} - \frac{v_z}{2c} \mathbf{A} + \frac{z}{2c} \mathbf{F} - \frac{\hat{e}_z}{2c} (\mathbf{v} \cdot \mathbf{A}) + \frac{\hat{e}_z}{2c} (\mathbf{r} \cdot \mathbf{F}), \quad (\text{B14})$$

we can obtain the velocities in the lab frame,

$$\mathbf{v}_{\perp, \text{lab}} = \mathbf{p}_\perp + \mathbf{A} + \frac{v_z}{2c} \mathbf{A} + \frac{z}{2c} \mathbf{F}, \quad (\text{B15})$$

$$v_{z, \text{lab}} = p_z + \frac{1}{2c} \left(\mathbf{p} \cdot \mathbf{A} + \frac{1}{2}A^2 \right) + \frac{1}{2c} \mathbf{r} \cdot \mathbf{F}. \quad (\text{B16})$$

At the tunnel exit, using $z \approx 0$ and

$$\begin{aligned} \mathbf{r}_0 &= \text{Re} \int_{t_s}^{t_r} \mathbf{v}_\perp dt = \text{Im} \int_0^{t_i} \left(1 + \frac{p_z}{2c} \right) \mathbf{A}(t_r + it) dt \\ &= -\frac{1}{2} t_i^2 \left(1 + \frac{p_z}{2c} \right) \mathbf{F}(t_r) \\ &\approx -\left(1 + \frac{p_z}{2c} \right) \frac{k_\perp^2 + 2I_p}{2} \frac{\mathbf{F}}{\tilde{F}^2}, \end{aligned} \quad (\text{B17})$$

we have $\mathbf{v}_{\perp, \text{lab}} = \mathbf{k}_\perp$, hence the mean initial linear momentum in the lab frame can be rewritten as

$$\begin{aligned} \langle v_z(t_r, v_\perp) \rangle_{E_2} &\approx \frac{2I_p + v_\perp^2}{4c} \left(1 + \frac{\mathbf{v}_\perp \cdot \dot{\mathbf{F}}(t_r)}{3F^2(t_r)} \right) \left(1 - \frac{2\alpha_Z F(t_r)}{(2I_p)^{3/2}} \right) \\ &\quad + \frac{F(t_r)}{4c\sqrt{2I_p}} \frac{F(t_r)}{F_d + F(t_r)} - \frac{2I_p + v_\perp^2}{4c} \frac{F^2(t_r)}{\tilde{F}^2(t_r)}, \end{aligned} \quad (\text{B18})$$

where we have dropped the subscript ‘‘lab’’, with the ponderomotive energy gain ΔE ,

$$\frac{\Delta E_{E_2}}{c} \approx \frac{p_\perp^2 - v_\perp^2}{4c} + \frac{2I_p + v_\perp^2}{4c} \frac{F^2(t_r)}{\tilde{F}^2(t_r)}, \quad (\text{B19})$$

and the corresponding asymptotic linear momentum

$$\begin{aligned} \langle p_z(t_r, v_\perp) \rangle_{E_2} &= \langle v_z(t_r, v_\perp) \rangle_{E_2} + \frac{\Delta E_{E_2}}{c} \\ &= \langle v_z(t_r, v_\perp) \rangle_{E_2} + \frac{p_\perp^2 - v_\perp^2}{4c} + \frac{2I_p + v_\perp^2}{4c} \frac{F^2(t_r)}{\tilde{F}^2(t_r)}. \end{aligned} \quad (\text{B20})$$

These results of Eqs. (B18–B20) are summarized in Table I.

Appendix C: F_1 term in the radiation gauge

The contribution of the field-linear term can be studied using the Hamiltonian in the radiation gauge containing only the F_1 term

$$H_{F_1} = \frac{1}{2} [\mathbf{p} + \mathbf{A}(t)]^2 + \frac{z}{c} \mathbf{F}(t) \cdot \mathbf{p} + V(r). \quad (\text{C1})$$

We carry out a gauge transformation with gauge phase $\Lambda = -(z/c) [\mathbf{p} \cdot \mathbf{A}(t)]$ to get a new Hamiltonian

$$H'_{F_1} = \frac{1}{2} \left[\mathbf{p} + \mathbf{A}(t) + \frac{\hat{e}_z}{c} \mathbf{p} \cdot \mathbf{A}(t) \right]^2 + V\left(r - \frac{z}{c} \mathbf{A}(t) \right), \quad (\text{C2})$$

where the corresponding saddle-point equation is written as

$$\frac{1}{2} \left[\mathbf{p} + \mathbf{A}(t_s) + \frac{\hat{e}_z}{c} \mathbf{p} \cdot \mathbf{A}(t_s) \right]^2 + I_p = 0. \quad (\text{C3})$$

In the ndSPA method, we define

$$\mathbf{k}_\perp = \left[\mathbf{p} + \left(1 - \frac{p_z}{c} \right) \text{Re} \mathbf{A}(t_s) \right] \cdot \frac{\text{Im} A_y(t_s) \hat{e}_x - \text{Im} A_x(t_s) \hat{e}_y}{\sqrt{(\text{Im} A_x(t_s))^2 + (\text{Im} A_y(t_s))^2}} \quad (\text{C4})$$

to obtain the linear momentum by evaluating Eq. (C3).

In the ndSPANE procedure, we may get

$$t_i = \sqrt{\frac{k_\perp^2 + 2I_p + p_z^2 + \frac{2p_z}{c} [2\mathbf{k}_\perp \cdot \mathbf{A}(t_r) - A^2(t_r)]}{\left[1 - \frac{p_z}{c} \frac{\mathbf{k}_\perp \cdot \dot{\mathbf{F}}(t_r)}{\tilde{F}^2(t_r)} \right] \tilde{F}^2(t_r)}}, \quad (\text{C5})$$

where $\mathbf{k}_\perp = \mathbf{p}_\perp + (1 - p_z/c) \mathbf{A}(t_r)$, with $\mathbf{k}_\perp \cdot \mathbf{F}(t_r) = 0$. Based on the exponential factor

$$\begin{aligned} 2\text{Im} S &= -2I_p t_i - \text{Re} \int_0^{t_i} \left[\mathbf{p} + \mathbf{A}(t_r + it) \right. \\ &\quad \left. + \frac{\hat{e}_z}{c} (\mathbf{p} \cdot \mathbf{A}(t_r + it)) \right]^2 dt \\ &\approx -\frac{2}{3\tilde{F}} \left[k_\perp^2 + 2I_p + \left(p_z \right. \right. \\ &\quad \left. \left. - \left(\frac{-2\mathbf{k}_\perp \cdot \mathbf{A} + A^2}{c} - \frac{2I_p + k_\perp^2}{6c} \frac{\mathbf{k}_\perp \cdot \dot{\mathbf{F}}}{\tilde{F}^2} \right) \right)^2 \right]^{\frac{3}{2}}, \end{aligned} \quad (\text{C6})$$

the preexponential prefactor

$$|\dot{S}|^{-\alpha z} \approx \left| -i \left(1 - \frac{p_z \mathbf{k}_\perp \cdot \dot{\mathbf{F}}}{c \tilde{F}^2} \right) t_i \tilde{F}^2 \right|^{-\alpha z} \\ \approx \left[(k_\perp^2 + 2I_p) \tilde{F}^2 \right]^{-\frac{\alpha z}{2}} \exp \left\{ -\frac{\alpha z}{2} \frac{p_z \mathbf{k}_\perp \cdot \dot{\mathbf{F}}}{c \tilde{F}^2} \right\} \\ \times \exp \left\{ -\frac{\alpha z}{2} \frac{\left(p_z - \frac{-2\mathbf{k}_\perp \cdot \mathbf{A} + A^2}{c} \right)^2}{k_\perp^2 + 2I_p} \right\}, \quad (\text{C7})$$

and the Jacobian

$$\left| \det \frac{\partial (p_x, p_y, p_z)}{\partial (t_r, k_\perp, p_z)} \right| \approx |F_d + F(t_r)| \left(1 - \frac{p_z}{c} \frac{F(t_r)}{F_d + F(t_r)} \right) \\ \approx |F_d + F(t_r)| \exp \left\{ -\frac{p_z}{c} \frac{F(t_r)}{F_d + F(t_r)} \right\}, \quad (\text{C8})$$

the transition rate is written as

$$\tilde{w}_{\text{ndSPANE}} \approx |F_d + F(t_r)| \left[(k_\perp^2 + 2I_p) \tilde{F}^2 \right]^{-\alpha z/2} \\ \times \exp \left\{ -\frac{2}{3\tilde{F}} \left[k_\perp^2 + 2I_p + \left(1 + \frac{\alpha z \tilde{F}}{2(k_\perp^2 + 2I_p)^{3/2}} \right) \right. \right. \\ \left. \left. \times (p_z - \langle p_z(t_r, k_\perp) \rangle_{F_1})^2 \right]^{3/2} \right\}, \quad (\text{C9})$$

where

$$\langle p_z(t_r, k_\perp) \rangle_{F_1} = -\frac{2I_p + k_\perp^2}{6c} \frac{\mathbf{k}_\perp \cdot \dot{\mathbf{F}}}{\tilde{F}^2} \left[1 - \frac{2\alpha z \tilde{F}}{(2I_p + k_\perp^2)^{3/2}} \right] \\ - \frac{\tilde{F}}{2c\sqrt{2I_p + k_\perp^2}} \frac{F}{F_d + F} + \frac{-2\mathbf{k}_\perp \cdot \mathbf{A} + A^2}{c} \\ \approx -\frac{2I_p + k_\perp^2}{6c} \frac{\mathbf{k}_\perp \cdot \dot{\mathbf{F}}}{F^2} \left[1 - \frac{2\alpha z F}{(2I_p)^{3/2}} \right] \\ - \frac{F}{2c\sqrt{2I_p}} \frac{F}{F_d + F} + \frac{-2\mathbf{k}_\perp \cdot \mathbf{A} + A^2}{c}. \quad (\text{C10})$$

According to the Heisenberg's equations of motion for $H_{F_1}^I$ [Eq. (C2)],

$$\mathbf{v}_\perp = \mathbf{p}_\perp + \mathbf{A} + \frac{p_z}{c} \mathbf{A}, \quad (\text{C11})$$

$$v_z = p_z + \frac{1}{c} \mathbf{p} \cdot \mathbf{A}, \quad (\text{C12})$$

and the frame transformation,

$$\mathbf{r}_{\text{lab}} = \mathbf{r} - \frac{z}{c} \mathbf{A}, \quad (\text{C13})$$

$$\mathbf{v}_{\text{lab}} = \mathbf{v} - \frac{v_z}{c} \mathbf{A} + \frac{z}{c} \dot{\mathbf{F}}, \quad (\text{C14})$$

we can obtain the velocities in the lab frame,

$$\mathbf{v}_{\perp, \text{lab}} = \mathbf{p}_\perp + \mathbf{A} + \frac{z}{c} \dot{\mathbf{F}}, \quad (\text{C15})$$

$$v_{z, \text{lab}} = p_z + \frac{1}{c} \mathbf{p} \cdot \mathbf{A}. \quad (\text{C16})$$

At the tunnel exit, using $z \approx 0$ we have

$$\mathbf{v}_{\perp, \text{lab}} = \mathbf{p}_\perp + \mathbf{A} \approx \mathbf{k}_\perp, \quad (\text{C17})$$

hence the mean initial linear momentum in the lab frame can be rewritten as

$$\langle v_z(t_r, v_\perp) \rangle_{F_1} \approx -\frac{2I_p + v_\perp^2}{6c} \frac{\mathbf{v}_\perp \cdot \dot{\mathbf{F}}(t_r)}{F^2(t_r)} \left[1 - \frac{2\alpha z F(t_r)}{(2I_p)^{3/2}} \right] \\ - \frac{F(t_r)}{2c\sqrt{2I_p}} \frac{F(t_r)}{F_d + F(t_r)} - \frac{\mathbf{v}_\perp \cdot \mathbf{A}(t_r)}{c}, \quad (\text{C18})$$

where we have dropped the subscript ‘‘lab’’, with the ponderomotive energy gain ΔE ,

$$\frac{\Delta E_{F_1}}{c} = \frac{-\mathbf{v}_\perp \cdot \mathbf{A}(t_r) + A^2(t_r)}{c}, \quad (\text{C19})$$

and the corresponding asymptotic linear momentum

$$\langle p_z(t_r, v_\perp) \rangle_{F_1} = \langle v_z(t_r, v_\perp) \rangle_{F_1} + \frac{\Delta E_{F_1}}{c} \\ = \langle v_z(t_r, v_\perp) \rangle_{F_1} - \frac{\mathbf{v}_\perp \cdot \mathbf{A}(t_r) - A^2(t_r)}{c}. \quad (\text{C20})$$

The results of Eqs. (C18–C20) are summarized in Table I.

Appendix D: F_2 term in the radiation gauge

The contribution of the field-quadratic term can be studied using the Hamiltonian in the radiation gauge containing only the F_2 term

$$H_{F_2} = \frac{1}{2} [\mathbf{p} + \mathbf{A}(t)]^2 + \frac{z}{c} \mathbf{A}(t) \cdot \dot{\mathbf{F}}(t) + V(\mathbf{r}). \quad (\text{D1})$$

We carry out a gauge transformation with gauge phase $\Lambda = -(z/2c)A^2(t)$ to get a new Hamiltonian

$$H'_{F_2} = \frac{1}{2} \left[\mathbf{p} + \mathbf{A}(t) + \frac{\hat{e}_z}{2c} A^2(t) \right]^2 + V(\mathbf{r}), \quad (\text{D2})$$

where the corresponding saddle-point equation is written as

$$\frac{1}{2} \left[\mathbf{p} + \mathbf{A}(t_s) + \frac{\hat{e}_z}{2c} A^2(t_s) \right]^2 + I_p = 0. \quad (\text{D3})$$

In the ndSPA method, we define

$$\mathbf{k}_\perp = \left[\mathbf{p} + \left(1 + \frac{p_z}{c} \right) \text{Re} \mathbf{A}(t_s) \right] \cdot \frac{\text{Im} A_y(t_s) \hat{e}_x - \text{Im} A_x(t_s) \hat{e}_y}{\sqrt{(\text{Im} A_x(t_s))^2 + (\text{Im} A_y(t_s))^2}} \quad (\text{D4})$$

to obtain the linear momentum by evaluating Eq. (D3).

In the ndSPANE procedure, we may get

$$t_i = \sqrt{\frac{k_{\perp}^2 + 2I_p + p_z^2 + \frac{2p_z}{c} \left(-\mathbf{k}_{\perp} \cdot \mathbf{A}(t_r) + \frac{1}{2}A^2(t_r) \right)}{\left[1 + \frac{p_z}{c} \left(1 + \frac{\mathbf{k}_{\perp} \cdot \tilde{\mathbf{F}}(t_r)}{\tilde{F}^2(t_r)} \right) \right] \tilde{F}^2(t_r)}}, \quad (\text{D5})$$

where $\mathbf{k}_{\perp} = \mathbf{p}_{\perp} + (1 + p_z/c)\mathbf{A}(t_r)$, with $\mathbf{k}_{\perp} \cdot \mathbf{F}(t_r) = 0$. Based on the exponential factor

$$\begin{aligned} 2\text{Im}S &= -2I_p t_i - \text{Re} \int_0^{t_i} \left[\mathbf{p} + \mathbf{A}(t_r + it) + \frac{\hat{e}_z}{2c} A^2(t_r + it) \right]^2 dt \\ &\approx -\frac{2}{3\tilde{F}} \left[k_{\perp}^2 + 2I_p + \left(p_z \right. \right. \\ &\quad \left. \left. - \left(\frac{\mathbf{k}_{\perp} \cdot \mathbf{A} - \frac{1}{2}A^2}{c} + \frac{2I_p + k_{\perp}^2}{6c} \left(1 + \frac{\mathbf{k}_{\perp} \cdot \tilde{\mathbf{F}}}{\tilde{F}^2} \right) \right) \right]^{\frac{3}{2}}, \end{aligned} \quad (\text{D6})$$

the preexponential prefactor

$$\begin{aligned} |\tilde{S}|^{-\alpha_Z} &\approx \left| -i \left[1 + \frac{p_z}{c} \left(1 + \frac{\mathbf{k}_{\perp} \cdot \tilde{\mathbf{F}}}{\tilde{F}^2} \right) \right] t_i \tilde{F}^2 \right|^{-\alpha_Z} \\ &\approx \left[(k_{\perp}^2 + 2I_p) \tilde{F}^2 \right]^{-\frac{\alpha_Z}{2}} \exp \left\{ -\frac{\alpha_Z}{2} \frac{p_z}{c} \left(1 + \frac{\mathbf{k}_{\perp} \cdot \tilde{\mathbf{F}}}{\tilde{F}^2} \right) \right\} \\ &\quad \times \exp \left\{ -\frac{\alpha_Z}{2} \frac{\left(p_z - \frac{\mathbf{k}_{\perp} \cdot \mathbf{A} - \frac{1}{2}A^2}{c} \right)^2}{k_{\perp}^2 + 2I_p} \right\}, \end{aligned} \quad (\text{D7})$$

and the Jacobian

$$\begin{aligned} \left| \det \frac{\partial(p_x, p_y, p_z)}{\partial(t_r, k_{\perp}, p_z)} \right| &\approx |F_d + F(t_r)| \left(1 + \frac{p_z}{c} \frac{F(t_r)}{F_d + F(t_r)} \right) \\ &\approx |F_d + F(t_r)| \exp \left\{ \frac{p_z}{c} \frac{F(t_r)}{F_d + F(t_r)} \right\}, \end{aligned} \quad (\text{D8})$$

the transition rate is written as

$$\begin{aligned} \tilde{w}_{\text{ndSPANE}} &\approx |F_d + F(t_r)| \left[(k_{\perp}^2 + 2I_p) \tilde{F}^2 \right]^{-\alpha_Z/2} \\ &\quad \times \exp \left\{ -\frac{2}{3\tilde{F}} \left[k_{\perp}^2 + 2I_p + \left(1 + \frac{\alpha_Z \tilde{F}}{2(k_{\perp}^2 + 2I_p)^{\frac{3}{2}}} \right) \right. \right. \\ &\quad \left. \left. \times (p_z - \langle p_z(t_r, k_{\perp}) \rangle_{F_2})^2 \right]^{\frac{3}{2}} \right\}, \end{aligned} \quad (\text{D9})$$

where

$$\begin{aligned} \langle p_z(t_r, k_{\perp}) \rangle_{F_2} &= \frac{2I_p + k_{\perp}^2}{6c} \left(1 + \frac{\mathbf{k}_{\perp} \cdot \tilde{\mathbf{F}}}{\tilde{F}^2} \right) \left[1 - \frac{2\alpha_Z \tilde{F}}{(2I_p + k_{\perp}^2)^{3/2}} \right] \\ &\quad + \frac{\tilde{F}}{2c\sqrt{2I_p + k_{\perp}^2}} \frac{F}{F_d + F} + \frac{\mathbf{k}_{\perp} \cdot \mathbf{A} - (1/2)A^2}{c} \\ &\approx \frac{2I_p + k_{\perp}^2}{6c} \left(1 + \frac{\mathbf{k}_{\perp} \cdot \tilde{\mathbf{F}}}{\tilde{F}^2} \right) \left[1 - \frac{2\alpha_Z F}{(2I_p)^{3/2}} \right] \\ &\quad + \frac{F}{2c\sqrt{2I_p}} \frac{F}{F_d + F} + \frac{\mathbf{k}_{\perp} \cdot \mathbf{A} - (1/2)A^2}{c}. \end{aligned} \quad (\text{D10})$$

Note that there is no translation to the origin in the Hamiltonian in the present case. According to the Heisenberg's equations of motion for H'_{F_2} [Eq. (D2)],

$$\mathbf{v}_{\perp, \text{lab}} = \mathbf{p}_{\perp} + \mathbf{A} \approx \mathbf{k}_{\perp}, \quad (\text{D11})$$

$$v_{z, \text{lab}} = p_z + \frac{1}{2c} A^2, \quad (\text{D12})$$

hence the mean initial linear momentum in the lab frame can be rewritten as

$$\begin{aligned} \langle v_z(t_r, v_{\perp}) \rangle_{F_2} &\approx \frac{2I_p + v_{\perp}^2}{6c} \left(1 + \frac{\mathbf{v}_{\perp} \cdot \tilde{\mathbf{F}}(t_r)}{F^2(t_r)} \right) \left[1 - \frac{2\alpha_Z F(t_r)}{(2I_p)^{3/2}} \right] \\ &\quad + \frac{F(t_r)}{2c\sqrt{2I_p}} \frac{F(t_r)}{F_d + F(t_r)} + \frac{\mathbf{v}_{\perp} \cdot \mathbf{A}(t_r)}{c}, \end{aligned} \quad (\text{D13})$$

where we have dropped the subscript "lab", with the ponderomotive energy gain ΔE ,

$$\frac{\Delta E_{F_2}}{c} = -\frac{1}{2c} A^2(t_r), \quad (\text{D14})$$

and the corresponding asymptotic linear momentum

$$\begin{aligned} \langle p_z(t_r, v_{\perp}) \rangle_{F_2} &= \langle v_z(t_r, v_{\perp}) \rangle_{F_2} + \frac{\Delta E_{F_2}}{c} \\ &= \langle v_z(t_r, v_{\perp}) \rangle_{F_2} - \frac{1}{2c} A^2(t_r). \end{aligned} \quad (\text{D15})$$

The results of Eqs. (D13–D15) are summarized in Table I.

From Table I, it is clear that the initial linear momentum $\langle v_z(t_r, v_{\perp}) \rangle$ can be decomposed into five contributions: the main contribution due to the exponential factor representing the under-barrier motion including the nondipole nonadiabatic coupling, the preexponential prefactor, the reduction factor caused by reducing the full nondipole Hamiltonian, the Jacobian factor introduced by the coordinate transformation $(p_x, p_y, p_z) \rightarrow (t_r, k_{\perp}, p_z)$, and the frame transformation factor mapping the nondipole frame to the lab frame. $\langle v_z \rangle$ is found in all cases to be modulated by the transverse tunneling momentum v_{\perp}^2 , which displays a subcycle variation due to nonadiabatic tunneling effects. Therefore, the interplay between nonadiabatic and nondipole tunneling effects results in a subcycle modulation of the linear momentum transfer at the tunnel exit as well of the asymptotic momentum transfer. The

TABLE II. Relationship between the initial momentum \mathbf{v}_\perp and the asymptotic momentum \mathbf{p}_\perp in the polarization plane under the individual nondipole Hamiltonian terms.

Terms	$\mathbf{v}_{\perp,\text{lab}}$
Total	$\mathbf{p}_\perp + \mathbf{A}(t_r)$
M ₁	$\mathbf{p}_\perp + \left(1 - \frac{p_z}{2c}\right) \mathbf{A}(t_r)$
E ₂	$\mathbf{p}_\perp + \left(1 + \frac{p_z}{2c}\right) \mathbf{A}(t_r)$
F ₁	$\mathbf{p}_\perp + \mathbf{A}(t_r)$
F ₂	$\mathbf{p}_\perp + \mathbf{A}(t_r)$

preexponential prefactor, arising partly from the nondipole transition element, is the same for all approximate Hamiltonians. Note that the reduction factor arises from separation of nondipole terms and appears only in the reduced Hamiltonians. Furthermore, the Jacobian and the frame transformations provide additive corrections only for these reduced Hamiltonians.

We note that when we treat different nondipole Hamiltonians, different relationships between the initial and asymptotic transverse momentum arise, which are summarized in Table II.

- [1] H. R. Reiss, The tunnelling model of laser-induced ionization and its failure at low frequencies, *J. Phys. B* **47**, 204006 (2014).
- [2] M.-X. Wang, S.-G. Chen, H. Liang, and L.-Y. Peng, Review on nondipole effects in ionization and harmonic generation of atoms and molecules, *Chin. Phys. B* **29**, 013302 (2020).
- [3] J. Maurer and U. Keller, Ionization in intense laser fields beyond the electric dipole approximation: concepts, methods, achievements and future directions, *J. Phys. B* **54**, 094001 (2021).
- [4] C. T. L. Smeenk, L. Arissian, B. Zhou, A. Mysyrowicz, D. M. Villeneuve, A. Staudte, and P. B. Corkum, Partitioning of the Linear Photon Momentum in Multiphoton Ionization, *Phys. Rev. Lett.* **106**, 193002 (2011).
- [5] A. Ludwig, J. Maurer, B. W. Mayer, C. R. Phillips, L. Gallmann, and U. Keller, Breakdown of the Dipole Approximation in Strong-Field Ionization, *Phys. Rev. Lett.* **113**, 243001 (2014).
- [6] F. Sun, X. Chen, W. Zhang, J. Qiang, H. Li, P. Lu, X. Gong, Q. Ji, K. Lin, H. Li, J. Tong, F. Chen, C. Ruiz, J. Wu, and F. He, Longitudinal photon-momentum transfer in strong-field double ionization of argon atoms, *Phys. Rev. A* **101**, 021402(R) (2020).
- [7] A. Hartung, S. Eckart, S. Brennecke, J. Ris, D. Trabert, K. Fehre, M. Richter, H. Sann, S. Zeller, K. Henrichs, G. Kastirke, J. Hoehl, A. Kalinin, M. S. Schöffler, T. Jahnke, L. P. H. Schmidt, M. Lein, M. Kunitski, and R. Dörner, Magnetic fields alter strong-field ionization, *Nat. Phys.* **15**, 1222 (2019).
- [8] S. Brennecke and M. Lein, High-order above-threshold ionization beyond the electric dipole approximation, *J. Phys. B* **51**, 094005 (2018).
- [9] K. Lin, S. Brennecke, H. Ni, X. Chen, A. Hartung, D. Trabert, K. Fehre, J. Rist, X.-M. Tong, J. Burgdörfer, L. Ph. H. Schmidt, M. S. Schöffler, T. Jahnke, M. Kunitski, F. He, M. Lein, S. Eckart, and R. Dörner, Magnetic-Field Effect in High-Order Above-Threshold Ionization, *Phys. Rev. Lett.* **128**, 023201 (2022).
- [10] P.-L. He, M. Klaiber, K. Z. Hatsagortsyan, and C. H. Keitel, Nondipole Coulomb sub-barrier ionization dynamics and photon momentum sharing, *Phys. Rev. A* **105**, L031102 (2022).
- [11] M. Klaiber, K. Z. Hatsagortsyan, and C. H. Keitel, Subcycle time-resolved nondipole dynamics in tunneling ionization, *Phys. Rev. A* **105**, 053107 (2022).
- [12] S. Brennecke and M. Lein, Nondipole modification of the ac Stark effect in above-threshold ionization, *Phys. Rev. A* **104**, L021104 (2021).
- [13] M. M. Lund and L. B. Madsen, Nondipole photoelectron momentum shifts in strong-field ionization with mid-infrared laser pulses of long duration, *J. Phys. B* **54**, 165602 (2021).
- [14] K. Lin, S. Eckart, A. Hartung, D. Trabert, K. Fehre, J. Rist, L. Ph. H. Schmidt, M. S. Schöffler, T. Jahnke, M. Kunitski, and Reinhard Dörner, Photoelectron energy peaks shift against the radiation pressure in strong-field ionization, *Sci. Adv.* **8**, eabn7386 (2022).
- [15] B. Willenberg, J. Maurer, B. W. Mayer, and U. Keller, Subcycle time resolution of multi-photon momentum transfer in strong-field ionization, *Nat. Commun.* **10**, 5548 (2019).
- [16] P. Eckle, M. Smolarski, P. Schlup, J. Biegert, A. Staudte, M. Schöffler, H. G. Muller, R. Dörner, and U. Keller, Attosecond angular streaking, *Nat. Phys.* **4**, 565 (2008).
- [17] P. Eckle, A. N. Pfeiffer, C. Cirelli, A. Staudte, R. Dörner, H. G. Muller, M. Büttiker, and U. Keller, Attosecond ionization and tunneling delay time measurements in helium, *Science* **322**, 1525 (2008).
- [18] A. Sommerfeld and G. Schur, Über den Photoeffekt in der K-Schale der Atome, insbesondere über die Voreilung der Photoelektronen, *Ann. Phys.* **396**, 409 (1930).
- [19] S. Chelkowski, A. D. Bandrauk, and P. B. Corkum, Photon Momentum Sharing between an Electron and an Ion in Photoionization: From One-Photon (Photoelectric Effect) to Multiphoton Absorption, *Phys. Rev. Lett.* **113**, 263005 (2014).
- [20] M. Klaiber, E. Yakaboylu, H. Bauke, K. Z. Hatsagortsyan, and C. H. Keitel, Under-the-Barrier Dynamics in Laser-Induced Relativistic Tunneling, *Phys. Rev. Lett.* **110**, 153004 (2013).
- [21] J. Liu, Q. Z. Xia, J. F. Tao, and L. B. Fu, Coulomb effects in photon-momentum partitioning during atomic ionization by intense linearly polarized light, *Phys. Rev. A* **87**, 041403(R) (2013).
- [22] S. Chelkowski, A. D. Bandrauk, and P. B. Corkum, Photon-momentum transfer in photoionization: From few photons to many, *Phys. Rev. A* **95**, 053402 (2017).
- [23] P.-L. He, D. Lao, and F. He, Strong Field Theories beyond Dipole Approximations in Nonrelativistic Regimes, *Phys. Rev. Lett.* **118**, 163203 (2017).
- [24] M.-X. Wang, X.-R. Xiao, H. Liang, S.-G. Chen, and L.-Y. Peng, Photon-momentum transfer in one- and two-photon ionization of atoms, *Phys. Rev. A* **96**, 043414 (2017).
- [25] S. V. B. Jensen, M. M. Lund, and L. B. Madsen, Nondipole strong-field-approximation Hamiltonian, *Phys. Rev. A* **101**, 043408 (2020).
- [26] L. B. Madsen, Nondipole effects in tunneling ionization by in-

- tense laser pulses, *Phys. Rev. A* **105**, 043107 (2022).
- [27] H. Ni, S. Brennecke, X. Gao, P.-L. He, S. Donsa, I. Březinová, F. He, J. Wu, M. Lein, X.-M. Tong, and J. Burgdörfer, Theory of Subcycle Linear Momentum Transfer in Strong-Field Tunneling Ionization, *Phys. Rev. Lett.* **125**, 073202 (2020).
- [28] N. Eicke, S. Brennecke, and M. Lein, Attosecond-Scale Streaking Methods for Strong-Field Ionization by Tailored Fields, *Phys. Rev. Lett.* **124**, 043202 (2020).
- [29] R. Anzaki, Y. Shinohara, T. Sato, and K. L. Ishikawa, Gauge invariance beyond the electric dipole approximation, *Phys. Rev. A* **98**, 063410 (2018).
- [30] H. Bachau and M. Dieng, Nondipole effects in helium ionization by intense soft x-ray laser pulses, *Eur. Phys. J. D* **73**, 123 (2019).
- [31] H. Liang, M.-X. Wang, X.-R. Xiao, Q. Gong, and L.-Y. Peng, Photon-momentum transfer in diatomic molecules: An ab initio study, *Phys. Rev. A* **98**, 063413 (2018).
- [32] A. Hartung, S. Brennecke, K. Lin, D. Trabert, K. Fehre, J. Rist, M. S. Schöffler, T. Jahnke, L. Ph. H. Schmidt, M. Kunitski, M. Lein, R. Dörner, and S. Eckart, Electric Nondipole Effect in Strong-Field Ionization, *Phys. Rev. Lett.* **126**, 053202 (2021).
- [33] G. F. Gribakin and M. Y. Kuchiev, Multiphoton detachment of electrons from negative ions, *Phys. Rev. A* **55**, 3760 (1997).
- [34] T. K. Kjeldsen and L. B. Madsen, Strong-field ionization of atoms and molecules: The two-term saddle-point method, *Phys. Rev. A* **74**, 023407 (2006).
- [35] D. B. Milošević, G. G. Paulus, D. Bauer, and W. Becker, Above-threshold ionization by few-cycle pulses, *J. Phys. B* **39**, R203 (2006).
- [36] S. P. Goreslavski and S. V. Popruzhenko, Differential photoelectron distributions in a strong elliptically polarized low-frequency laser field, *Sov. Phys. JETP* **83**, 661 (1996).
- [37] N. I. Shvetsov-Shilovski, S. V. Popruzhenko, and S. P. Goreslavski, Asymmetric emission of rescattered photoelectrons in intense laser fields with elliptical polarization, *Laser Phys.* **13**, 1054 (2003).
- [38] S. P. Goreslavski, G. G. Paulus, S. V. Popruzhenko, and N. I. Shvetsov-Shilovski, Coulomb asymmetry in above-threshold ionization, *Phys. Rev. Lett.* **93**, 233002 (2004).
- [39] M. V. Frolov, N. L. Manakov, A. A. Minina, S. V. Popruzhenko, and A. F. Starace, Adiabatic-limit Coulomb factors for photoelectron and high-order-harmonic spectra, *Phys. Rev. A* **96**, 023406 (2017).
- [40] H. Ni, N. Eicke, C. Ruiz, J. Cai, F. Oppermann, N. I. Shvetsov-Shilovski, and L.-W. Pi, Tunneling criteria and a nonadiabatic term for strong-field ionization, *Phys. Rev. A* **98**, 013411 (2018).
- [41] Y. Ma, J. Zhou, P. Lu, H. Ni, and J. Wu, Influence of nonadiabatic, nondipole and quantum effects on the attoclock signal, *J. Phys. B* **54**, 144001 (2021).
- [42] M. Ohmi, O. I. Tolstikhin, and T. Morishita, Analysis of a shift of the maximum of photoelectron momentum distributions generated by intense circularly polarized pulses, *Phys. Rev. A* **92**, 043402 (2015).
- [43] K. Liu, S. Luo, M. Li, Y. Li, Y. Feng, B. Du, Y. Zhou, P. Lu, and I. Barth, Detecting and Characterizing the Nonadiabaticity of Laser-Induced Quantum Tunneling, *Phys. Rev. Lett.* **122**, 053202 (2019).